

# Structural Properties of $\text{Sn}_x\text{S}_y$ Thin Films Prepared by Plasma-Enhanced Chemical Vapor Deposition

A. Sanchez-Juarez<sup>a</sup> and A. Ortiz<sup>b</sup>

<sup>a</sup>Department of Solar Materials, Energy Research Center, Universidad Nacional Autonoma de Mexico, Temixco, Morelos, 62580 Mexico

<sup>b</sup>Materials Research Institute, Universidad Nacional Autonoma de Mexico, Coyoacan, D. F., 04510 Mexico

The growth and structural properties of  $\text{Sn}_x\text{S}_y$  ( $\text{SnS}_2$ ,  $\text{Sn}_2\text{S}_3$ ) prepared by the plasma-enhanced chemical vapor deposition process have been studied systematically.  $\text{Sn}_x\text{S}_y$  thin films were prepared by the decomposition of  $\text{H}_2\text{S}$  and  $\text{SnCl}_4$  vapors mixture in a capacitively coupled 13.56 MHz radio frequency glow discharge chamber with a radially symmetric flow pattern. Hydrogen was used as a diluent gas and for removing chlorine radicals generated by the  $\text{SnCl}_4$  decomposition. The deposition pressure, substrate temperature, and plasma power density were kept constant at 50 mTorr, 150°C, and 25 mW/cm<sup>2</sup>, respectively. The relative concentration of the precursor materials,  $g$ , defined as the ratio of tin chloride mass flow rate to the sum of tin chloride and hydrogen sulfide mass flow rates, was varied from 0 to 1.0. A total mass flow rate of 25 standard cubic centimeter per minute for the precursor materials and the diluent gas was used in all the cases. It was found that (i) For  $g < 0.2$ , the deposited thin films contain only the 2H-SnS<sub>2</sub> phase, and show a hexagonal crystalline structure with a preferential growth of the  $c$  axes perpendicular to the plane of the substrate; (ii) For  $0.2 \leq g < 0.5$ , and  $g > 0.6$ , the deposited films contain a mixture of hexagonal SnS<sub>2</sub> and orthorhombic Sn<sub>2</sub>S<sub>3</sub> compounds; and (iii) For  $g$  close to 0.5, the deposited material has only the Sn<sub>2</sub>S<sub>3</sub> compound. In all the samples, the size of the crystallites and the lattice parameters were estimated from the width of the X-ray diffraction peaks and the interplanar distances. It was found that the chemical composition, the crystallinity, and the preferential growth of the deposited material are well controlled by adjusting the value of  $g$ .

© 2000 The Electrochemical Society. S0013-4651(00)02-060-7. All rights reserved.

Manuscript submitted February 15, 2000; revised manuscript received July 3, 2000.

Binary compounds like SnS, SnS<sub>2</sub>, and Sn<sub>2</sub>S<sub>3</sub>, based on Sn and S, are semiconductor materials<sup>1-3</sup> with a high potential use in optoelectronic devices due to their optical and electrical properties.<sup>4-6</sup> These semiconductors have been prepared by different processes such as chemical melt growth,<sup>3,7-9</sup> chemical vapor transport,<sup>10,11</sup> physical vapor transport,<sup>12</sup> chemical vapor deposition (CVD),<sup>13</sup> electroless deposition,<sup>14</sup> spray pyrolysis,<sup>15-17</sup> and glow discharge.<sup>18</sup> The structural, optical, and electrical properties of the different compounds in the binary Sn-S system depend on the preparation technique.

Tin sulfide, SnS, crystallizes into a deformed NaCl structure, which is described to be composed of tightly bonded double layers of Sn and S atoms along the  $c$  axis, with van der Waals-type binding between layers.<sup>19</sup> The single crystalline material has shown indirect transitions with an optical bandgap of about 1.3 eV,<sup>3</sup> which lies in the optimum range for absorber materials to be used in solar cells applications.<sup>20</sup> It is a p-type material whose conductivity can be increased by doping with Ag, Al, N, and Cl.<sup>3,21</sup> On the other hand, polycrystalline thin films have an optical bandgap in the range of 1.1 to 1.3 eV.<sup>13</sup>

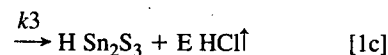
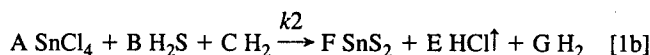
Tin disulfide, SnS<sub>2</sub>, is a layered compound that crystallizes in the hexagonal CdI<sub>2</sub>-type structure with at least three basic polytypes that are classified in terms of their stacking sequence.<sup>22</sup> The basic structure unit represented by  $(A_\gamma B)_n$  is called 2H-SnS<sub>2</sub>, where  $\gamma$  corresponds to Sn, and A and B correspond to the S layers. SnS<sub>2</sub> single crystals have shown an n-type electrical conductivity,<sup>23</sup> and optical bandgaps in the range of 2.12 to 2.44 eV.<sup>7,10-11</sup> Sn<sup>II</sup>Sn<sup>IV</sup>S<sub>3</sub> is classified as a Type I mixed valence compound. This material shows semiconductor behavior with an energy bandgap dependent of its crystalline structure and stoichiometry. Thin film polycrystalline samples of Sn<sub>2±x</sub>S<sub>3</sub> present allowed indirect optical transitions with an optical bandgap ranging from 1.16 to 1.9 eV.<sup>13,15,16</sup>

Taking into account the optoelectronic properties of Sn and S-based compounds, it can be inferred that these materials could be used to build photovoltaic p-n or p-i-n structures with a conversion efficiency of about 25%.<sup>20</sup> These structures should be low cost devices because the materials involved are inexpensive, nonstrategic, and abundant in nature. However, in order to create a cost-competitive photovoltaic cell, it is necessary to have a precisely, controllable, simple, and inexpensive large area thin film deposition technique. The plasma-enhanced chemical vapor deposition (PECVD), is a

process that meets these requirements. In order to use these materials in a thin film device, it is important to know their structural properties and their dependence on the preparation conditions. To our knowledge, only a few papers have been devoted to the study of the structural properties of  $\text{Sn}_x\text{S}_y$  polycrystalline thin film materials, and in only one, the PECVD process was used. Recently Ortiz *et al.*<sup>18</sup> have reported the deposition of p-type SnS polycrystalline thin films by PECVD. The present work deals with the deposition of  $\text{Sn}_x\text{S}_y$  thin films by PECVD. Here, growth and structural properties are analyzed as a function of the concentration ratio of the source materials. An optimization of the deposition parameters to grow SnS<sub>2</sub> and Sn<sub>2</sub>S<sub>3</sub> thin film materials is also presented.

## Experimental

**The chemical reaction.**—From a mixture of SnCl<sub>4</sub> and H<sub>2</sub>S vapors diluted with H<sub>2</sub>, depending on the mole ratio of the reactants and external stimulants, different sulfides of tin can be formed in the following reactions



The values of A, B...H, vary with the reactants and products of the particular reaction and are related to the number of moles involved, while  $k_1$ ,  $k_2$ ,  $k_3$  are the unknown reaction rate constants. The reactants in the left side of Eq. 1 could produce the products in the right side if the reaction is activated by means of external energy.

**Thin film preparation.**—Sn<sub>x</sub>S<sub>y</sub> thin films were prepared in a glow discharge system with a radially symmetric flow pattern. A 13.56 MHz radio frequency (rf) generator with a matching network drives the glow discharge onto a capacitively coupled planar electrode configuration. Figure 1 shows a schematic diagram of the system. To control the gas flow rate of the precursor vapors (SnCl<sub>4</sub> and H<sub>2</sub>S) and the diluent gas (H<sub>2</sub>) electronic mass flow controllers were used. The deposition pressure was measured by a baratron and it was controlled automatically with a throttle valve. Two kinds of substrates

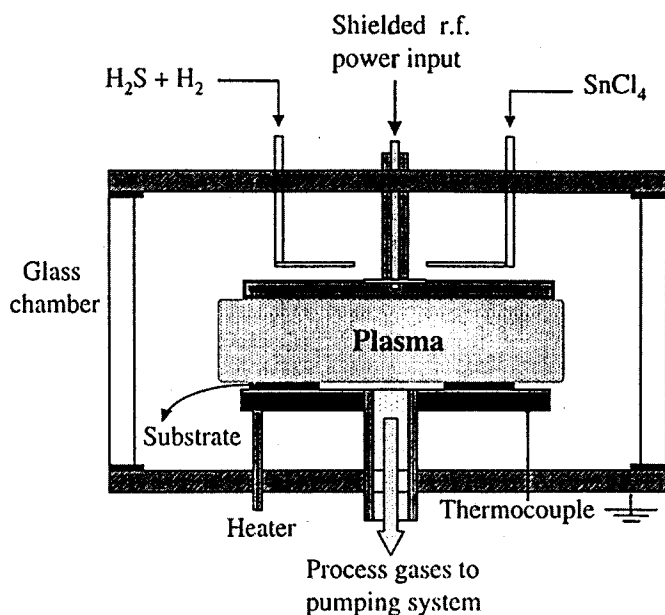


**Figure 1.** Schematic diagram of the PECVD chamber with a radially symmetric flow pattern. A fixed distance of 3 cm separates the two circular electrode plates with a diam of 16 cm.

were used: Pyrex glass slices, chemically and ultrasonically cleaned and 200  $\Omega$  cm n-type (100) single crystal silicon wafers, both with  $1.5 \times 2.5$  cm area. The flow rates of the precursors were chosen to meet a maximum flow rate of 5 standard cubic centimeter per minute (sccm) for the  $\text{SnCl}_4$  and  $\text{H}_2\text{S}$  mixture. The liquid  $\text{SnCl}_4$  vapor source was kept at  $40^\circ\text{C}$  in all cases. The substrate temperature was controlled by means of a temperature controller at a fixed value of  $150^\circ\text{C}$  through a K-type thermocouple. The plasma power density and the process pressure were kept constant at  $0.025 \text{ W/cm}^2$  and 50 mTorr, respectively. The concentration rate of the precursors,  $g$ , defined by the following relation

$$g = \frac{[\text{SnCl}_4]}{[\text{SnCl}_4] + [\text{H}_2\text{S}]} \quad [2]$$

was varied from 0.0 to 1.0 in 0.1 steps. The square brackets in Eq. 2 indicate the flow rate in sccm.  $\text{H}_2$  was added at a flow rate of 20 sccm as a diluent gas. The total gas flow rate for  $\text{H}_2$ ,  $\text{SnCl}_4$ , and  $\text{H}_2\text{S}$  was 25 sccm in all cases.

**Film characterization.**—The thickness of the deposited films on glass was measured with an Alpha Step 100 profilometer. The crystal structure was analyzed by X-ray diffraction (XRD) measurements on a Siemens D-500 diffractometer using  $\text{Cu K}\alpha$  radiation of  $\lambda = 1.5405 \text{ \AA}$ . The diffraction patterns were taken with a scan rate of  $2\theta = 0.5/\text{min}$ . Surface morphology was observed by scanning electron microscopy (SEM) using Cambridge-Leica Stereoscan 440 SEM equipment. The composition of the film was determined by the energy dispersive spectroscopy (EDS) analysis using an Oxford system detector attached to the scanning electron microscope.

### Results and Discussion

**Primary processes.**—In a glow discharge process, the electrons are the principal sources for transferring electrical energy to the gas molecules through elastic and inelastic collisions that lead and contribute to a variety of chemical reactions.<sup>24</sup> Among them, the excitation and deexcitation processes produce the glow. Hence, it is important to know the gas-pressure and electric power to be used in order to produce the desired gas discharge breakdown in the reaction chamber.

The physical conditions necessary to produce and sustain a glow discharge plasma using either  $\text{SnCl}_4$ ,  $\text{H}_2\text{S}$ , or  $\text{H}_2$  for the chamber shown in Fig. 1 were investigated separately. The flow rates of  $\text{SnCl}_4$  and  $\text{H}_2\text{S}$  vapors were fixed at 5 sccm, while that of  $\text{H}_2$  was fixed at 20 sccm. The minimum rf power required for the breakdown of the

plasma, as a function of the gas pressure in the chamber is shown in Fig. 2. The grounded plate was at room temperature in all cases. For each gas there exists a minimum value for the rf power that depends on the gas pressure. This value is related to the minimum energy required to the breakdown. This behavior can be explained considering that at low pressure the electron mean free path ( $\lambda_e$ ) is large, and thus the majority of the electrons reach the electrodes without colliding with gas molecules. Therefore, the lower the pressure, the higher is the value of rf power needed to produce the breakdown of the gas. On the other hand,  $\lambda_e$  becomes short at higher pressures. In this case, electrons can not gain a high enough energy from the ac electric field to ionize the gas because of their frequent collisions with the gas molecules. Thus, rf power increases as the pressure increases. By analogy with the Paschen curve of a dc plasma,<sup>25</sup> the left side of the minimum in Fig. 2 is called the low pressure regime and the right side, the high pressure regime. The rf power needed to sustain the plasma is lower than the one needed to the breakdown of the plasma. This is explained by the fact that once the plasma starts, electrons and ions are trapped in the discharge space. These electrons frequently cause ionization of gas molecules by inelastic collisions, then the rf power needed to sustain the plasma decreases from its initial value to a value that keeps the rate of generation and recombination of electrons balanced.<sup>25</sup> Figure 2 also shows that  $\text{H}_2\text{S}$  requires less rf power for starting the glow than the others, in range of pressure considered. This behavior could be understood considering that the energy needed to produce an excitation state in a molecule is lower than the one required to produce an ionization state. Since the ionization potential of the  $\text{H}_2\text{S}$  molecule (10.45 eV) is lower than those of  $\text{SnCl}_4$  (11.88 eV) and  $\text{H}_2$  (15.42 eV) molecules,<sup>26</sup> it can be expected that the molecule that requires less energy for having an ionization state will require less energy for having an excited state. Thus, the  $\text{H}_2\text{S}$  molecule has an excitation state at relatively less rf power than the others.

In order to know if there are reactions besides excitation and deexcitation processes, the solid materials deposited onto glass substrates in the low pressure regime of Fig. 2 for  $\text{SnCl}_4$  alone, the  $\text{SnCl}_4/\text{H}_2$  mixture and  $\text{H}_2\text{S}$  discharges were investigated under the following conditions: process pressure of 50 mTorr; rf power of 5 W (power density of  $25 \text{ mW/cm}^2$ ), and deposition time of 30 min. Two substrate temperatures were used: 35 and  $150^\circ\text{C}$ , to analyze the possible effects of this parameter on the decomposition of the precursors.

**The  $\text{SnCl}_4$  discharge.**—Figure 3a shows the XRD patterns of the solid materials deposited at 35 and  $150^\circ\text{C}$ , showing diffraction peaks

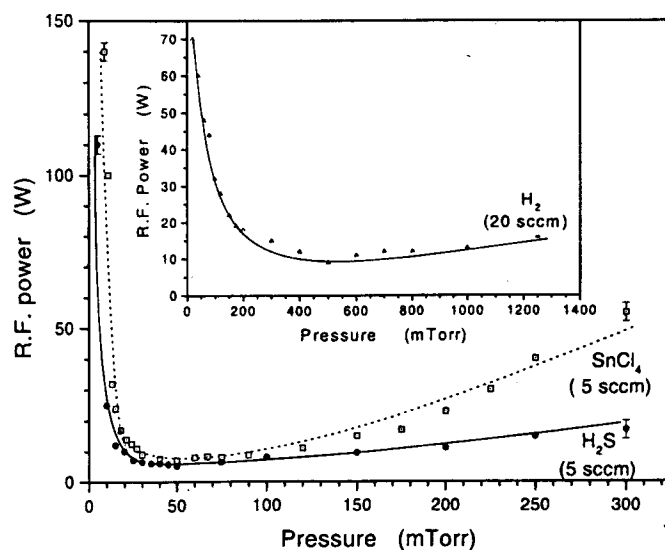


**Figure 2.** Behavior of the gas discharge breakdown for the vapor precursors and  $\text{H}_2$ . Tin tetrachloride and hydrogen sulfide are fed down into the chamber at a rate of 5 sccm, while hydrogen is fed at 20 sccm.

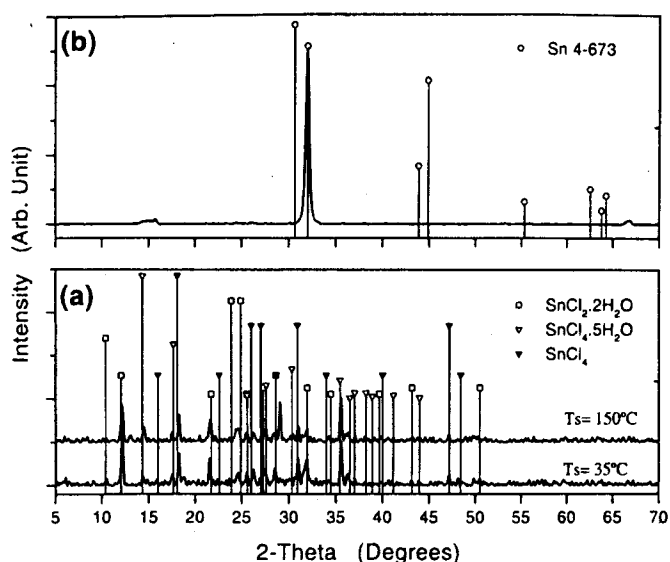
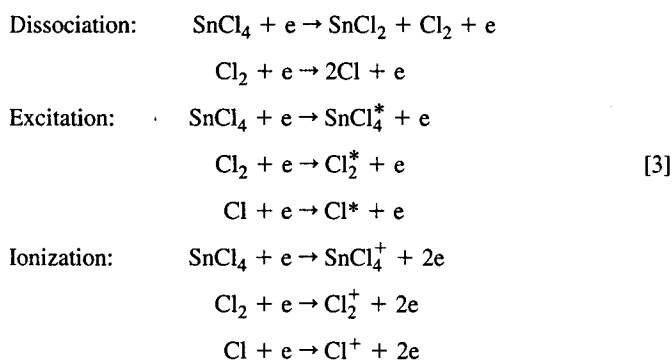
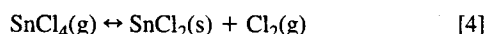


**Figure 3.** XRD patterns of a material deposited on a glass substrate using a rf power of 5 W, substrate temperatures of 35 and 150°C, and plasma generated by vapors of SnCl<sub>4</sub>. The upper pattern corresponds to a material deposited when hydrogen was used as a diluent in a proportion 1:4 of SnCl<sub>4</sub>/H<sub>2</sub>.

attributable to SnCl<sub>4</sub>, SnCl<sub>4</sub>·5H<sub>2</sub>O, and SnCl<sub>2</sub>·2H<sub>2</sub>O (JCPDS no. 31-1394, 31-1395, and 32-1380, respectively), all polycrystalline materials. No other compound could be identified with these peaks, and no peak due to elemental Sn was identified in the patterns. Thus, at these conditions, SnCl<sub>4</sub> is not decomposed into Sn and Cl radicals. The chemical processes that could take place due to electron-molecule collisions, but not limited to them, are represented by (→) in Eq. 3, where e denotes the electron. These processes suggest that a significant amount of free Cl, Cl<sub>2</sub>, and different tin chloride radicals will be produced during the deposition as by-products of the dissociation of SnCl<sub>4</sub>

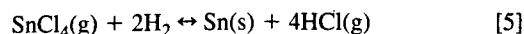


Further experiments like mass spectrometry and optical emission spectroscopy should be carried out in order to know the ionic and luminescent species that can be associated with the possible reactions. Another reaction that can be associated with the formation of a solid film is the condensation of SnCl<sub>4</sub> vapors onto the glass substrate via the reaction<sup>13</sup>

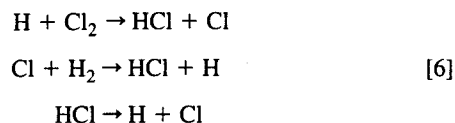


On the other hand, this experiment did not show evidence that the substrate temperature enhances the SnCl<sub>4</sub> decomposition in the temperature range considered.

**The SnCl<sub>4</sub>/H<sub>2</sub> discharge.**—When hydrogen was used as a diluent, in a proportion 1:4 of SnCl<sub>4</sub>/H<sub>2</sub>, the material deposited was only metallic tin as indicated by the XRD pattern in Fig. 3b. This result can be explained on the basis of hydrogen being considered as a strong reducing agent. Then, the following overall reaction takes place



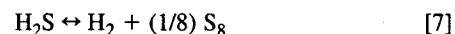
Also, the H<sub>2</sub> species produced by the plasma like H<sub>2</sub><sup>\*</sup> (excited molecules), H (atoms), H<sup>\*</sup> (excited atoms), H<sub>2</sub><sup>+</sup> (ions), and H<sup>+</sup> (protons),<sup>24</sup> could be responsible for this overall chemical reaction in chain reactions of the type expressed in Eq. 6



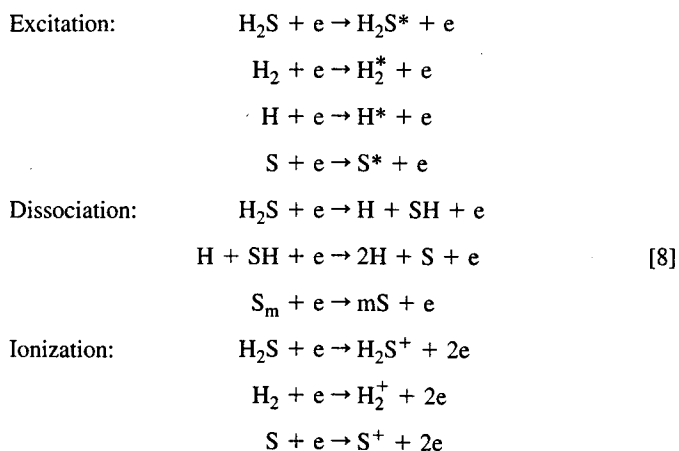
Furthermore, for producing Sn<sub>x</sub>S<sub>y</sub> thin films without chlorine incorporation, hydrogen added to the reaction could remove Cl atoms from the gas phase and even from the growing film. It is seen from Eq. 1 that the presence of H<sub>2</sub> in the mixture reduces Sn<sup>4+</sup> to Sn<sup>2+</sup>. In addition, it can combine with the Cl present in the system to form HCl. Thus, the extraction of Cl during the deposition process of these thin films can be controlled by the amount of hydrogen added to the reaction chamber. It is important to note that an excess of H<sub>2</sub> per each SnCl<sub>4</sub> molecule is necessary for extracting as much chlorine as possible. This behavior has been studied for chlorinated SiO<sub>2</sub> thin films prepared by PECVD. In this case Alonso *et al.*<sup>27</sup> found that it is necessary to add a H<sub>2</sub> flow rate more than twice that of the precursor flow rate, in order to eliminate Cl incorporation in the film. In the present work, it is expected that Cl incorporation will be avoided since the flow rate of H<sub>2</sub> to that of the precursor was set at four.

When a high power density, *i.e.*, 500 mW/cm<sup>2</sup>, was used to produce the glow discharge, it was found that the deposited material has incorporated compounds related to SnCl<sub>2</sub> and metallic tin, hence the SnCl<sub>4</sub> is decomposed into Sn and Cl radicals.

**The H<sub>2</sub>S discharge.**—For the substrate at a temperature of 35°C, the deposited thin film showed a yellow color in reflection that could be associated with solid sulfur formed by the decomposition of H<sub>2</sub>S.<sup>28</sup> There was no film deposition at a substrate temperature of 150°C. This can be explained as follows: at room temperature, the generated sulfur is condensed and adsorbed on the substrate surface with a residence time long enough to form a thin film. At 150°C, the adsorbed sulfur acquires the necessary energy to be desorbed with a high desorption rate. Thus, sulfur is returned to the plasma generating more active species. In the case of the material deposited at low temperature, the XRD pattern did not show any diffraction peak that could be attributed to sulfur. This may be due to the small thickness of the film or perhaps due to the amorphous nature of the deposited material. The overall reaction<sup>28</sup> that could take place is given by



caused by one or more of the following processes, represented by (→) in Eq. 8, derived from electron-molecule collisions, but not limited to them



Thus, in the low pressure regime, H<sub>2</sub>S is decomposed due to inelastic collisions with electrons in the plasma. However, SnCl<sub>4</sub> is not decomposed by the electron-molecule collision.<sup>24</sup> This result is a direct consequence of the energy required to break a chemical bond. The H-S bond needs 3.57 eV, while Cl-Sn needs 4.29 eV.<sup>26</sup>

**Deposition of Sn<sub>x</sub>S<sub>y</sub> thin films.**—Figure 4 shows the behavior of the rf power against pressure to establish the breakdown plasma process in a 1:1 mixture of SnCl<sub>4</sub> and H<sub>2</sub>S, with and without H<sub>2</sub> dilution. In both cases, there is a minimum in the curve that defines the concept of low pressure and high pressure regime, in agreement with Paschen's curve. It can be seen that H<sub>2</sub> enhances the breakdown at pressures higher than 150 mTorr, in a similar way as is shown in the inset of Fig. 2; while at pressure lower than 150 mTorr, the mixture of H<sub>2</sub>S and SnCl<sub>4</sub> breaks down more readily.

In the present study, all of the deposited Sn<sub>x</sub>S<sub>y</sub> thin films were carried out using deposition parameters in the low pressure regime. Therefore, there is no primary decomposition of SnCl<sub>4</sub> by the plasma and the chemical reactions that lead to thin film growth must be related to the H<sub>2</sub>S decomposition and the reduction of SnCl<sub>4</sub> by H<sub>2</sub>.

**Deposition rate.**—Figure 5 shows the behavior of the deposition rate ( $R_d$ ), defined by the thickness divide by deposition time, as a function of  $g$ , for samples prepared at a deposition time of 30 min. Each point represents the mean value of  $R_d$  for at least six samples prepared at the same conditions and located at the same position on the grounded electrode. The error bars in each point show the experimental standard deviation for the  $R_d$  mean value. In this figure, the  $g$  range is divided into five regions. In regions I and II,  $R_d$  increases as  $g$  increases. In region III,  $R_d$  decreases up to a minimum value for  $g \approx 0.6$ ; after which,  $R_d$  increases as  $g$  increases up to about  $g = 0.7$ . Region IV shows a saturation behavior of  $R_d$  with  $g$ ; and finally in region V when  $g = 1$ ,  $R_d$  drops to a very low value. To explain this behavior it is necessary to analyze the deposited material. Thus, XRD and EDS analyses were performed in samples with similar thickness ( $\approx 0.15 \mu\text{m}$ ).

**Structural and compound identification.**—Figure 6 shows the XRD patterns of typical samples prepared for  $g < 0.2$  (region I). Peak identification was performed following the procedure described in Ref. 29. The observed peaks match with those of the standard pattern for tin disulfide (2H-SnS<sub>2</sub>; JCPDS no. 23-677). This compound has a hexagonal structure lying in the space group  $P3m1$ . The strong peak located at  $2\theta$  around  $15^\circ$  is due to reflections from the (001) plane. The appearance of the [001] strong peak indicates that the deposited material is highly oriented with the  $c$  axes perpendicular to the plane of the substrate. This type of growth is a

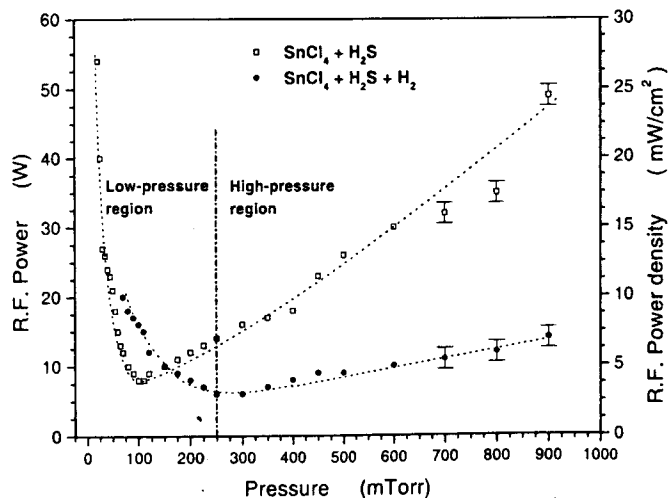


Figure 4. Gas discharge breakdown behavior for a mixture 1:1 of SnCl<sub>4</sub> and H<sub>2</sub>S: curve (□) without hydrogen dilution, and curve (●) with hydrogen dilution.

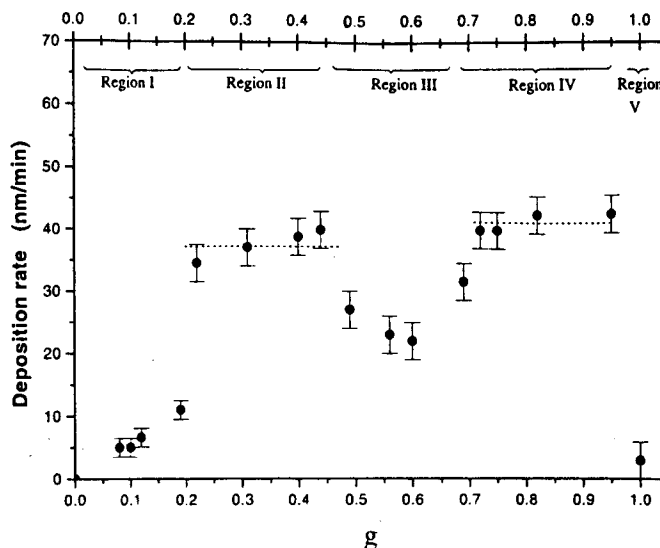


Figure 5. Behavior of the deposition rate as a function of  $g$ . Regions I, II, III, IV, and V are defined by the intervals shown on the top of this figure.

common feature for single crystal SnS<sub>2</sub> prepared by chemical vapor transport.<sup>30</sup> To our knowledge, no one else has reported this kind of growth for polycrystalline SnS<sub>2</sub> thin films. Prominent peaks, the calculated grain size, and their corresponding  $d$  values for these SnS<sub>2</sub> thin films are listed and compared with those of the standard patterns in Table I. The  $2\theta$  peak position in each pattern is shifted to lower values as  $g$  increases. This behavior could be attributed to the inclusion of chlorine impurities in the SnS<sub>2</sub> lattice or to slight departures from the stoichiometry of the compound, *i.e.*, a metal to sulfur ratio greater than 1:2. Both hypotheses are supported later. The lattice parameters found are in close agreement with the reported values for the standard powder samples of SnS<sub>2</sub>, and they are similar to those reported for single crystals of SnS<sub>2</sub> prepared by other processes (see for instance, Kourtakis *et al.*<sup>11</sup> and Ray *et al.*<sup>31</sup>). It can be seen from Table I that the lattice parameter  $c$  experiences a slight increase as  $g$  increases, and its mean value is 1.2% higher than the standard one. This small discrepancy is also associated with the same cause that has been proposed to explain the small shift in the  $2\theta$  peak position observed in the patterns of Fig. 6. Therefore, in region I, an increase in  $g$  does not affect the preferential growth of the films and the lattice parameters of the SnS<sub>2</sub> crystal. On the other hand, the magni-

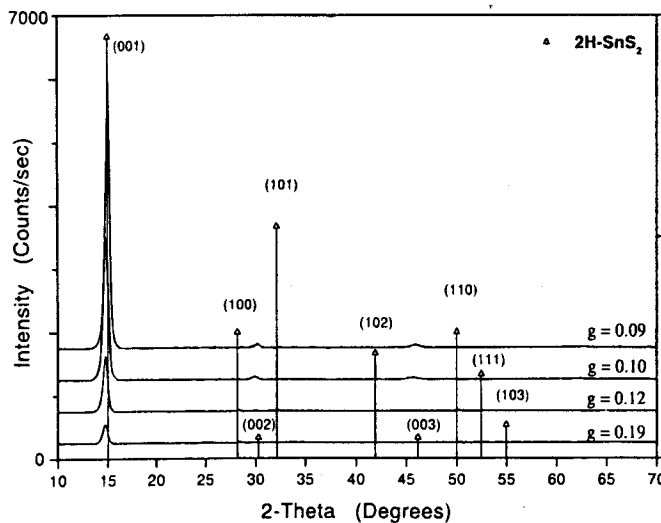


Figure 6. Typical XRD patterns for samples prepared using  $g \leq 0.2$ . All the patterns show a strong peak for the (001) planes, indicating preferred orientation along [001].

**Table I. Prominent peak positions ( $2\theta$  values) of XRD peaks, corresponding  $d$ -values,  $g$ s, lattice parameters, and their identification as 2H-SnS<sub>2</sub> for samples prepared with  $g < 0.2$ .**

$g$	Phase	Observation Sn <sub>x</sub> S <sub>y</sub> polycrystalline thin films (Strong peak positions)				Lattice parameters			Comparison 2H-SnS <sub>2</sub> (JCPDS data file 23-677) Systematic hexagonal; Lattice parameters: $a = 3.649 \text{ \AA}$ ; $c = 5.899 \text{ \AA}$			
		Peak ( $2\theta$ )	$d$ -value ( $\text{\AA}$ )	$hkl$	$g$ s (nm)	$a$	$b$	$c$	Peak ( $2\theta$ )	$d$ -value ( $\text{\AA}$ )	$hkl$	( $hkl$ )
0.09	SnS <sub>2</sub>	15.07	5.879	100	16			5.913	15.029	5.89	100	(001)
		30.22	2.960	2					30.262	2.951	5	(002)
0.1	SnS <sub>2</sub>	14.83	5.969	100	14			5.966	15.029	5.89	100	(001)
		29.85	2.99	2					30.262	2.951	5	(002)
0.12	SnS <sub>2</sub>	14.81	5.981	100	13	3.639		5.981	15.029	5.89	100	(001)
		28.31	3.148	3					28.199	3.162	30	(100)
0.19	SnS <sub>2</sub>	14.76	6.002	100	13	3.637		6.002	15.029	5.89	100	(001)
		28.35	3.145	7					28.199	3.162	30	(100)

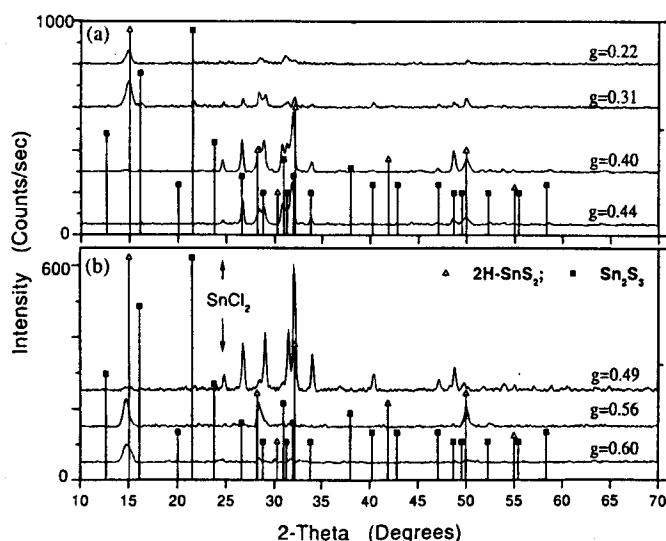
tudes of the reflection peak at  $2\theta = 15.03^\circ$  decreases as  $g$  increases (see Fig. 6). The crystallite size calculated using these peaks decreases slightly as  $g$  increases, showing a trend toward a mean value of 13 nm (see Table I). This reduction could also be associated to the inclusion of chlorine impurities at the crystal network in the sulfur position.

Figure 7 shows the X-ray diffractograms for typical samples prepared at  $g$  values corresponding to region II (Fig. 7a) and to region III (Fig. 7b). Peak positions of each one of these patterns were compared with the standard JCPDS data file card no. 23-677 for 2H-SnS<sub>2</sub> and card no. 14-619 for Sn<sub>2</sub>S<sub>3</sub>. Figure 7a shows peaks that correspond to the 2H-SnS<sub>2</sub> and Sn<sub>2</sub>S<sub>3</sub> compounds. Therefore, the identification procedure confirmed that both compounds grew simultaneously in this interval of  $g$ , while only the Sn<sub>2</sub>S<sub>3</sub> is deposited when  $g$  takes a value close to 0.49. This fact is confirmed in Fig. 7b in which all the peak positions in the spectra corresponding to  $g = 0.49$ , except the two at  $2\theta \approx 24.9$  and  $40.3^\circ$ , match the standard for the Sn<sub>2</sub>S<sub>3</sub> compound. The peaks at  $2\theta \approx 24.9$  and  $40.3^\circ$  are associated with the SnCl<sub>2</sub>·2H<sub>2</sub>O compound (see Fig. 3a). Using a similar chamber and under similar deposition conditions, except for the deposition pressure ( $g = 0.5$  and a deposition pressure of 150 mTorr), Ortiz *et al.*<sup>18</sup> found that the deposited material was SnS. In the present work, all the samples were

prepared using a deposition pressure of 50 mTorr, which is below the threshold value found in Fig. 4, and there is no evidence of the SnS compound in all the deposited films. This difference could be attributed to the deposition pressure that gives another reaction path. The deposition pressure is an important parameter that must be taken into consideration. Similar results have been observed for a-Si:H and a-SiC:H thin films produced by PECVD.<sup>32,33</sup>

As  $g$  increases, taking values in region III, Sn<sub>2</sub>S<sub>3</sub> apparently stops growing and the SnS<sub>2</sub> compound grows again with the hexagonal crystal structure, in a similar way as those prepared using  $g$  values within the interval (0.12, 0.31). This is evident from Fig. 7b in which the XRD patterns corresponding for samples grown using  $g = 0.56$  and 0.6 show strong peaks corresponding to the SnS<sub>2</sub> compound, meanwhile the peaks corresponding to the Sn<sub>2</sub>S<sub>3</sub> almost disappear. There are other weak peaks in the patterns shown in Fig. 7, but the signal-to-noise ratio of those peaks is very small. All the samples prepared within the interval (0.2, 0.49) do not show any preferential growth like that observed for the SnS<sub>2</sub> compound. Prominent peaks, corresponding  $d$  values, grain size ( $g$ s), lattice parameters, and their respective assignments for samples prepared within  $0.2 < g \leq 0.6$  are listed and compared in Table II.

Figure 8 shows the XRD patterns for samples prepared using  $g$  values in region IV. There are big peaks corresponding to 2H-SnS<sub>2</sub> and SnCl<sub>2</sub>·2H<sub>2</sub>O, and small peaks located around  $2\theta \approx 12.8^\circ$  and  $38^\circ$  that corresponded to the Sn<sub>2</sub>S<sub>3</sub> (see Fig. 8a). In Fig. 8b, there are peaks other than those which could be associated with the 4H-SnS<sub>2</sub> phase (polytype of the 2H-SnS<sub>2</sub> with double  $c$  axes),  $\beta$ -S, and metallic tin (JCPDS no. 21-1231, 34-0941, and 4-673, respectively). The last assignment was done because for  $g = 1$ , the deposited material was metallic tin (see Fig. 3b). The peak corresponding to 4H-SnS<sub>2</sub> at  $2\theta \approx 29.2^\circ$  was only observed for  $g > 0.72$ , means that as  $g$  increases, the 2H is gradually transformed into the 4H structure. The reverse behavior has been observed for tin disulfide single crystal grown by chemical vapor transport.<sup>30</sup> Prominent peaks and their corresponding  $d$  values for the deposited thin films prepared using  $g$  values within the considered interval ( $0.6 < g \leq 1$ ) are listed and compared in Table III. There is a small shift in all the diffraction peak positions with respect to the standard peak position considered in Tables II and III. This behavior is due to the fact that both SnS<sub>2</sub> and Sn<sub>2</sub>S<sub>3</sub> compounds are grown along with SnCl<sub>2</sub>. Tables II and III also show that the crystalline  $g$ s for the 2H-SnS<sub>2</sub> phase, calculated using the peak at  $2\theta \approx 15^\circ$ , almost remains constant with a mean value of 12.8 nm for all  $g$  values except for  $g > 0.75$  for which it is of the order of 28 nm. The latter is calculated using the peak at  $2\theta \approx 29.2^\circ$ . This difference in the crystalline grain size can be associated with the change in the size of the lattice parameters, because the deposited material is identified as the 4H-SnS<sub>2</sub> phase. The Sn<sub>2</sub>S<sub>3</sub>



**Figure 7.** XRD patterns for samples prepared using discrete  $g$  values from 0.22 up to 0.6. These patterns show how the crystal structures are changing as  $g$  increases.

**Table II. Prominent peak positions (2θ values) of XRD peaks, corresponding d-values, gs, lattice parameters, and their respective identification, for samples prepared with 0.2 < g ≤ 0.6.**

g	Phase	Observation Sn <sub>x</sub> S <sub>y</sub> polycrystalline thin films (Strong peak positions)				Lattice parameters			Comparison 2H-SnS <sub>2</sub> (JCPDS data file 23-677) Systemic Hexagonal; Lattice parameters: a = 3.649 Å; c = 5.899 Å				Comparison Sn <sub>2</sub> S <sub>3</sub> (JCPDS data file 14-619) Systemic Orthorhombic; Lattice parameters: a = 8.864 Å; b = 14.020 Å; c = 3.747 Å			
		Peak (2θ)	d-value (Å)	l//o	gs (nm)	a	b	c	Peak (2θ)	d-value (Å)	l//o	(hkl)	Peak (2θ)	d-value (Å)	l//o	(hkl)
0.22	SnS <sub>2</sub>	14.89	5.932	100	12	3.638	—	5.932	15.029	5.89	100	(001)	—	—	—	—
	Sn <sub>2</sub> S <sub>3</sub>	31.14	2.875	100	14	8.653	13.836	3.847	—	—	—	—	30.916	2.89	5	(310)
0.31	SnS <sub>2</sub>	14.98	5.921	100	13	3.638	—	5.921	15.029	5.89	100	(001)	—	—	—	—
	Sn <sub>2</sub> S <sub>3</sub>	21.66	4.094	100	17	8.778	13.885	3.757	—	—	—	—	21.498	4.13	100	(130)
0.40	SnS <sub>2</sub>	28.36	3.144	100	13	3.637	—	5.806	28.199	3.162	30	(100)	—	—	—	—
	Sn <sub>2</sub> S <sub>3</sub>	31.90	2.804	100	20	8.923	13.754	3.738	—	—	—	—	31.936	2.80	15	(211)
0.44	SnS <sub>2</sub>	28.37	3.143	100	13	3.629	—	5.80	28.199	3.162	30	(100)	—	—	—	—
	Sn <sub>2</sub> S <sub>3</sub>	31.82	2.811	100	19	8.888	14.142	3.73	—	—	—	—	31.936	2.80	15	(211)
0.49	Sn <sub>2</sub> S <sub>3</sub>	32.11	2.785	100	28	8.853	13.907	3.709	—	—	—	—	31.936	2.80	15	(211)
0.60	SnS <sub>2</sub>	14.73	6.012	100	13	3.638	—	6.012	15.029	5.89	100	(001)	—	—	—	—

compound did not show any preferential growth and the crystalline grain size calculated at the peak position considered shows an increasing trend as g increases up to 0.69, after that, the grain size tends to a value of 30 nm.

**Surface morphology and composition.**—Figure 9 shows typical SEM micrographs of Sn<sub>x</sub>S<sub>y</sub> thin films prepared using different g values. The surface appearance changes from smooth to rough as g increases. For g > 0.2, the micrographs show crystal grains comprised of randomly oriented wormlike structures or fibrils. The fibrils appeared to be larger for g > 0.6 than those for g < 0.6. This surface appearance could be related to the crystalline phase of the material: SnS<sub>2</sub> for g < 0.2 and a mixture of SnS<sub>2</sub> and Sn<sub>2</sub>S<sub>3</sub> compounds with inclusion of crystallites of SnCl<sub>2</sub> for g > 0.2. A very smooth surface is obtained for the SnS<sub>2</sub> compound, while a rough surface is observed for the mixture. The latter could be attributed to the growth competition between the SnS<sub>2</sub> and Sn<sub>2</sub>S<sub>3</sub> compounds, and the deposition of SnCl<sub>2</sub> occurring for g > 0.2. Similar features, like those

shown in Fig. 9 have been found also for Sn<sub>x</sub>S thin film prepared by low temperature chemical precipitation, dip deposition, and cathodic electrodeposition.<sup>13,31,34</sup>

The composition of the deposited Sn<sub>x</sub>S<sub>y</sub> thin films, determined by EDS analyses, can be used to determine the stoichiometry of the compound. The atomic percentage (atom %) of Sn, S, and Cl incorporated in the deposited material as a function of g are shown in Fig. 10. It can be seen that for g < 0.2 and for g = 0.6, the atomic percentage of Sn and S incorporated are almost in the ratio of Sn/S = 0.5, thus the stoichiometry of the thin films was found to be 1:2, which confirms the formation of the SnS<sub>2</sub> compound. This is in agreement with the compound identified by XRD. In the case of g = 0.09, it was found that the ratio Sn/S ≈ 0.17, meaning that the deposited material has a significant Sn deficiency. Thus, the stoichiometry is of the form Sn<sub>1-x</sub>S<sub>2</sub>. On the other hand, it was not possible to define a unique stoichiometry for 0.2 < g < 0.95, except for 0.6, because the deposited material is formed by two compounds. The quantity of Sn incorporated remains almost constant with a value around 40 atom %, while the quantity of S is almost 55 atom %, then for g = 0.49 the ratio 40 atom % Sn to 55 atom % S is approximately in the ratio 2:3, that identifies the Sn<sub>2</sub>S<sub>3</sub> compound. Also, it can be seen that there is chlorine incorporation in the deposited material for all the g values, except for g < 0.1.

The atom % of Cl shows a small increasing trend as g increases, and its maximum concentration is less than 5 atom % even for g = 1. There are two ways in which Cl can be incorporated in the deposited material: as a tin chloride related radical, as a SnCl<sub>2</sub>-like compound as has been identified in XRD (see Fig. 7 and 8), or as an impurity replacing sulfur. The inclusion of atomic Cl in the deposited material as an impurity instead of sulfur (the ionic radius of chloride is less than that of the sulfide), or as a compound, could be responsible for the shift of the peak position of the XRD patterns shown in Fig. 6, 7, and 8, as well as for the deviation of the values in the lattice parameters of the deposited material.<sup>29</sup> In the case of SnS<sub>2</sub>, the Cl incorporation could affect the electrical properties of the films, as has been shown in previous works.<sup>3,21</sup> Although the Cl concentration found is small, the quantity of H<sub>2</sub> added to the reaction or the deposition conditions was not enough to leave a chlorine free Sn<sub>x</sub>S<sub>y</sub> network.

**Formation process.**—It was found that the precursor concentration, represented by g, affects the chemical composition of the deposited material, giving SnS<sub>2</sub> thin films for g < 0.2, and thin films with a mixture of Sn<sub>2</sub>S<sub>3</sub> and SnS<sub>2</sub> for g > 0.2. In order to explain how

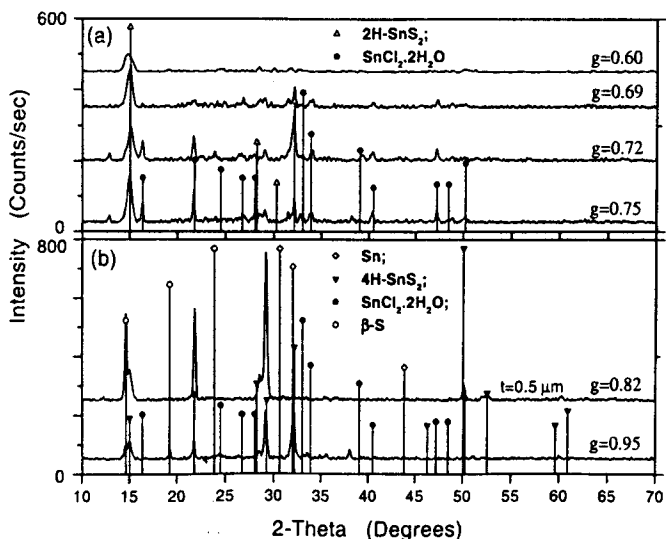


**Figure 8. XRD patterns for samples prepared with g ≥ 0.6. The peak at 2θ ≈ 29.2° confirms the gradual transformation of the 2H-SnS<sub>2</sub> into the 4H-SnS<sub>2</sub> structure.**

**Table III. Prominent peak positions ( $2\theta$  values) of XRD peaks, corresponding  $d$ -values,  $g$ s, lattice parameters, and their respective identification for samples prepared with  $g > 0.6$ .**

Observation $\text{Sn}_x\text{S}_y$ polycrystalline thin films (Strong peak positions)										Comparison $2\text{H-SnS}_2$ (JCPDS data file 23-677) Systematic hexagonal; Lattice parameters: $a = 3.649 \text{ \AA}; c = 5.899 \text{ \AA}$				Comparison $\text{Sn}_2\text{S}_3$ (JCPDS data file 14-619) Systematic Orthorhombic; Lattice parameters: $a = 8.864 \text{ \AA}; b = 14.020 \text{ \AA}; c = 3.747 \text{ \AA}$			
$g$	Phase	Peak ( $2\theta$ )	$d$ -value ( $\text{\AA}$ )	$hkl$	$g$ s (nm)	Lattice parameters			Peak ( $2\theta$ )	$d$ -value ( $\text{\AA}$ )	$hkl$	( $hkl$ )	Peak ( $2\theta$ )	$d$ -value ( $\text{\AA}$ )	$hkl$	( $hkl$ )	
						$a$	$b$	$c$									
0.69	$\text{SnS}_2$	15.04	5.894	100	12	3.645	—	5.894	15.029	5.89	100	(001)					
	$\text{Sn}_2\text{S}_3$	26.79	3.324	100	46	8.849	13.895	3.711	—	—	—	—	23.586	3.35	15	(111)	
0.72	$\text{SnS}_2$	15.10	5.866	100	13	3.604	—	5.866	15.029	5.89	100	(001)					
	$\text{Sn}_2\text{S}_3$	21.77	4.086	100	25	8.754	13.903	3.733	—	—	—	—	21.498	4.13	100	(130)	
0.75	$\text{SnS}_2$	14.99	5.910	100	13	3.646	—	5.91	15.029	5.89	100	(001)					
	$\text{Sn}_2\text{S}_3$	21.73	4.088	100	31	8.763	13.841	3.774					21.498	4.13	100	(130)	
										Comparison $4\text{H-SnS}_2$ (JCPDS data file 21-231) Systematic Hexagonal; Lattice parameters: $a = 3.645 \text{ \AA}; c = 11.802 \text{ \AA}$				Comparison $\text{Sn}_2\text{S}_3$ (JCPDS data file 14-619) Systematic Orthorhombic; Lattice parameters: $a = 8.864 \text{ \AA}; b = 14.020 \text{ \AA}; c = 3.747 \text{ \AA}$			
$g$	Phase	Peak ( $2\theta$ )	$d$ -value ( $\text{\AA}$ )	$hkl$	$g$ s (nm)	Lattice parameters			Peak ( $2\theta$ )	$d$ -value ( $\text{\AA}$ )	$hkl$	( $hkl$ )	Peak ( $2\theta$ )	$d$ -value ( $\text{\AA}$ )	$hkl$	( $hkl$ )	
						$a$	$b$	$c$									
0.82	$\text{SnS}_2$	29.19	3.059	100	28	3.623	—	11.79	29.257	3.05	16	(101)					
	$\text{Sn}_2\text{S}_3$	21.86	4.065	100	27	8.203	14.04	3.734					21.498	4.13	100	(130)	
0.95	$\text{SnS}_2$	29.22	3.062	100	29	3.614	—	11.79	29.257	3.05	16	(101)					
	$\text{Sn}_2\text{S}_3$	21.82	4.074	100	28	8.943	13.909	3.689					21.498	4.13	100	(130)	
										Comparison Sn (JCPDS data file 4-673) Systematic Tetragonal; Lattice parameters: $a = 5.831 \text{ \AA}; c = 3.182 \text{ \AA}$							
$g$	Phase	Peak ( $2\theta$ )	$d$ -value ( $\text{\AA}$ )	$hkl$	$g$ s (nm)	Lattice parameters			Peak ( $2\theta$ )	$d$ -value ( $\text{\AA}$ )	$hkl$	( $hkl$ )					
						$a$	$b$	$c$									
1.0	Sn	32.0	2.795	100	18	5.831	—	3.225	32.018	2.793	90	(101)					

the formation of these compounds occurs, it is supposed that all the molecules that are fed down to the chamber undergo a chemical reaction. Since all the processes were carried out in the low pressure regime, the primary decomposition products are radicals related with

$\text{H}_2\text{S}$ , probably atomic and molecular sulfur, meanwhile, the  $\text{SnCl}_4$  vapor reacts with  $\text{H}_2$  and with those radicals generated by the  $\text{H}_2\text{S}$  decomposition mainly via ionic reactions. During the glow discharge of the gases  $\text{SnCl}_4$ ,  $\text{H}_2\text{S}$ , and  $\text{H}_2$ , some of the processes pre-

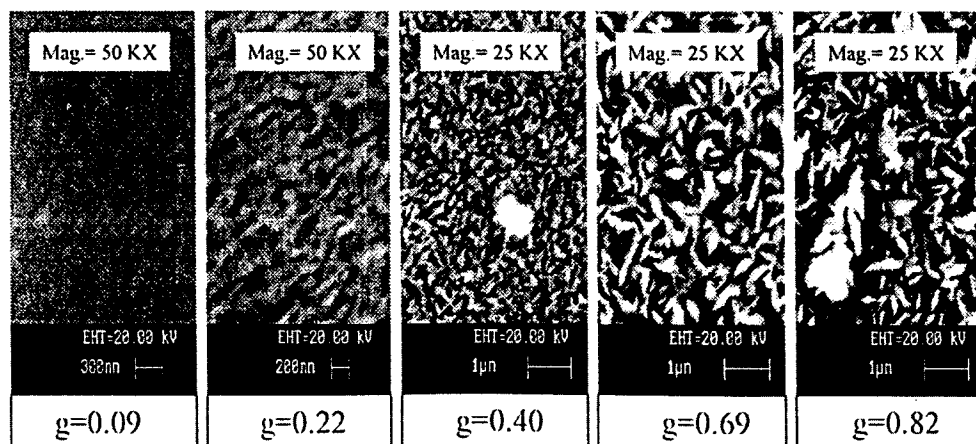


**Figure 9.** SEM micrographs showing the morphology of the  $\text{Sn}_x\text{S}_y$  thin film compounds deposited at different  $g$  values. It is clear that the surface morphology changes from smooth to rough as  $g$  increases.

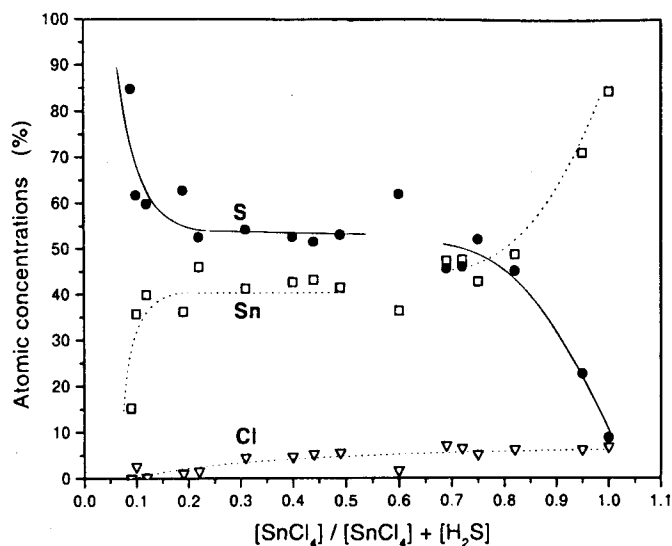
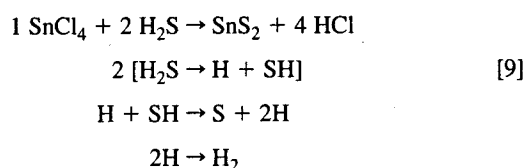


Figure 10. Sn, S, and Cl atomic concentrations incorporated at the thin films as a function of the precursor concentration.

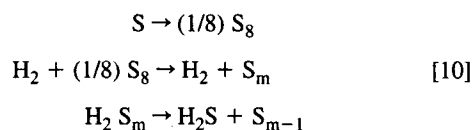
sented in Eq. 3 to 8 will produce the products and reactions represented in Table IV. Thus, the  $\text{Sn}_x\text{S}_y$  compound formation could be explained on the basis of the processes described below.

**$\text{SnS}_2$  formation.**—When  $g \leq 0.2$ , the atomic concentration of S inside the reaction chamber before starting the glow discharge is higher than that of Sn. For example, for  $g = 0.2$ , for each atom of tin there are four atoms of S, and the concentration of S increases as  $g$  decreases. This argument holds because it is well known that the mass flow rate measured in sccm is proportional to the number of molecules per minute that is flowing to the reaction chamber. The relationship is given by  $1 \text{ sccm} = 2.69 \times 10^{19}$  molecules per minute.<sup>35</sup> Following the work by Engelken *et al.*,<sup>13</sup> for growing thin films of tin disulfide, it is necessary to have one  $\text{Sn}^{4+}$  ion and  $2\text{S}^{2-}$  ions to produce Reaction d in Table IV. Because  $\text{Sn}^{2+}$  could be formed by the reduction of  $\text{SnCl}_2$  with  $\text{H}_2$ , the  $\text{Sn}^{4+}$  ion is obtained by Reaction b in Table IV. Then, if all the  $\text{SnCl}_4$  molecules produce the  $\text{Sn}^{4+}$  ions, there are more than twice as many atoms of S in the reaction chamber, for producing the  $\text{S}^{2-}$  ion to form the  $\text{SnS}_2$  compound. The overall chemical reactions yielding the formation of  $\text{SnS}_2$  thin films could be the following

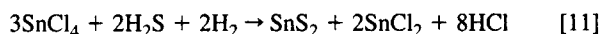


The  $\text{H}_2$  molecules flowing inside the reaction chamber at a flow rate of 20 sccm are not represented in these balanced equations, but a cer-

tain number of them react with  $\text{SnCl}_4$  to produce the above mentioned reactions. Since XRD patterns for  $g < 0.2$  did not show evidence of atomic sulfur in the deposited thin film, there must exist another reaction path involved during the process besides the one represented in this equation. Thus, it was assumed that  $\text{H}_2\text{S}$  is generated during the glow discharge, after the initial dissociation of the inlet  $\text{H}_2\text{S}$  through the following reactions



This assumption is supported by Traus *et al.*,<sup>36</sup> These authors showed the production of  $\text{H}_2\text{S}$  from the dissociation of a mixture of  $\text{H}_2/\text{H}_2\text{S}$  in a high pressure glow discharge. This process occurs when the relative concentration of  $\text{H}_2$  in the mixture is higher than that of the  $\text{H}_2\text{S}$  by a factor of 2.33. In our case, the  $\text{H}_2/\text{H}_2\text{S}$  ratio is higher than this value. Therefore, although the concentration of  $\text{H}_2\text{S}$  is higher than the concentration of  $\text{SnCl}_4$ , it is possible to suppose that only 50% of the molecules of the hydrogen sulfide are involved in the reaction to produce the  $\text{SnS}_2$  material, while the rest react in the way shown in Eq. 10. It was also found that for  $g \approx 0.6$  the deposited material shows mainly the  $\text{SnS}_2$  compound. Under this condition, before starting the glow discharge, the atomic concentration of Sn is 1.5 times that of S. Then it is expected that the following reaction takes place



Though according to the stoichiometry of the reaction, only 10% of  $\text{H}_2$  introduced to the chamber is required for the reaction shown in Eq. 11, it was observed that thin films of  $\text{SnS}_2$  are formed only when an excess of  $\text{H}_2$  is present. Equation 11 explains the presence of  $\text{SnCl}_2$  in the deposited thin film. The XRD pattern for the samples prepared with  $g = 0.6$  (see Fig. 7b) shows peaks attributed to  $\text{SnCl}_2 \cdot 2\text{H}_2\text{O}$ . Water molecules are attached to  $\text{SnCl}_2$  because this compound absorbs water when the deposited thin films are exposed to the atmosphere.

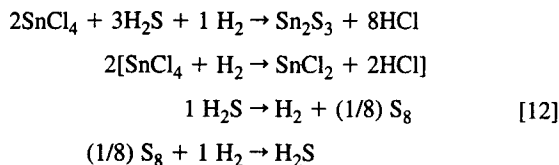
**$\text{Sn}_2\text{S}_3$  formation.**—In the presence of  $\text{S}^{2-}$  and  $\text{SnCl}_2$  molecules, the  $\text{Sn}_2\text{S}_3$  compound can be formed through Reaction c in Table IV, requiring four molecules of  $\text{SnCl}_2$  with three molecules of S to produce one molecule of  $\text{Sn}_2\text{S}_3$  and two molecules of  $\text{SnCl}_4$ .<sup>13</sup> Regarding the effect of the concentration of the precursors on the structure and composition of the films (see Table II), the  $\text{Sn}_2\text{S}_3$  compound was obtained only in the case of samples prepared with a  $g$  value around 0.5, where the atomic concentrations of S and Sn in the reaction chamber are the same before starting the glow. If it is assumed that all the  $\text{SnCl}_4$  molecules are transformed to  $\text{SnCl}_2$ , then only 75% of the atomic sulfur generated by the decomposition of the  $\text{H}_2\text{S}$  molecules is necessary for the chemical balance of Reaction c on Table IV. Under this condition, out of the 100% of the  $\text{SnCl}_2$  molecules that are involved in this chemical reaction, 50% react with S to

Table IV. Precursors, by-products, and reactions that could take place in a PECVD process using  $\text{SnCl}_4$  and  $\text{H}_2\text{S}$  compound like precursors for growing  $\text{Sn}_x\text{S}_y$  thin film materials.

Precursors and diluent	By-products	Reactions in the presence of hydrogen and/or sulfur
$\text{SnCl}_4$	$\text{SnCl}_2, \text{Cl}_2;$ $\text{Sn}, \text{HCl}$	(a) $\text{SnCl}_2$ yields $\text{Sn}^{2+}$ and $\text{Cl}^-$ (b) Disproportionation of $\text{Sn}^{2+}$ yields $\text{Sn}^{4+}$ and Sn (c) $\text{SnCl}_2$ and S yields $\text{Sn}_2\text{S}_3$ and $\text{SnCl}_4$
$\text{H}_2\text{S}$	$\text{H}_2^+, \text{H}^+, \text{S}, \text{S}_2,$ $\text{S}^{2-}, \text{S}_2^2-$	(d) $\text{Sn}^{4+}$ and $2\text{S}^{2-}$ yields $\text{SnS}_2$ (e) Sn and $\text{S}_m$ yields $\text{SnS}_x$ and $\text{S}_{m-x}$ (f) $\text{SnCl}_2, \text{S}$ and $\text{H}_2^+$ yields $\text{SnS}$ and $\text{HCl}$
$\text{H}_2$	$\text{H}, \text{H}_2^+$	(g) $\text{SnS}$ and S yields $\text{SnS}_2$ (h) $\text{Sn}_2\text{S}_3$ and S yields $\text{SnS}_2$



form the  $\text{Sn}_2\text{S}_3$  compound and the other 50% form  $\text{SnCl}_4$  again. The overall reactions that could take place is given by



which can continue until the S concentration goes down. At this limit, the formation of  $\text{SnCl}_2$  is expected. This explains the incorporation of  $\text{SnCl}_2$  in the deposited material prepared for  $g = 0.49$  (see Fig. 7b).

In the region of  $0.2 < g < 0.5$ , the atomic concentration of sulfur is higher than that of tin before starting the glow. During the glow, the chemical reaction represented in Eq. 12 takes place, but due to the fact that there are more S than Sn, part of the generated S are adsorbed on the growing  $\text{Sn}_2\text{S}_3$  thin film surface yielding the formation of  $\text{SnS}_2$  through the reaction



Thus, since not all of the  $\text{Sn}_2\text{S}_3$  material is transformed into  $\text{SnS}_2$ , the  $\text{Sn}_2\text{S}_3$ - $\text{SnS}_2$  mixture may be produced. This explanation supports our results obtained for  $0.2 < g < 0.49$  for which the deposited material presents both compounds.

In the case of  $0.6 < g < 1$ , the reaction chamber has more molecules of Sn than S. Then the following reactions could take place.

1. Reduction of  $\text{SnCl}_4$  by  $\text{H}_2$  giving  $\text{SnCl}_2$  and HCl.
2. Decomposition of  $\text{H}_2\text{S}$  into  $\text{H}_2$  and  $\text{S}_m$  through a reaction such as Eq. 10.
3. A reaction of  $\text{SnCl}_2$  with  $\text{S}_m$  to form  $\text{SnS}_2$  and by-products like  $\text{SnCl}_2$ , HCl,  $\text{H}_2$ , and  $\text{S}_{m-2}$ .

All these reactions take place until  $g$  goes to 1. Therefore, it is possible to obtain a solid thin film material formed by several compounds, mainly  $\text{SnS}_2$  and  $\text{SnCl}_2$  for  $0.6 < g < 0.75$ ; and  $\text{SnS}_2$ , S,  $\text{SnCl}_2$ , and even metallic Sn for  $g > 0.75$ , as can be seen in Fig. 8a and b.

On the other hand, during the plasma process, tin ions ( $\text{Sn}^{4+}$ ,  $\text{Sn}^{2+}$ ) and atomic Sn, produced by the reduction of  $\text{SnCl}_4$ , coexist at the same time with ions of sulfur ( $\text{S}^{2-}$ ), and it is expected that SnS compound could be generated through Reaction f in Table IV. Nevertheless, XRD did not show evidence of this material in the deposited thin films. This observation does not exclude the formation of SnS. Perhaps the excess of S present will react with SnS to form  $\text{SnS}_2$ , in the same way as with  $\text{Sn}_2\text{S}_3$ .<sup>13</sup> Thus, the stoichiometry of the deposited film is shifted toward  $\text{SnS}_2$  as has been shown in the present study.

Since there are several reactions that yield to different compounds in the range of  $g$  chosen in the present study, the dynamics of the growth process strongly depends on the concentrations of the precursors. Their effect would be reflected in  $R_d$  as well. Based on the results obtained and considering that the films are deposited by an atomic (molecular) growth process (typical in PECVD), it is possible to explain the behavior of  $R_d$  shown in Fig. 5, as follows.

**Region I.**—When the  $\text{SnCl}_4$  concentration increases, the atomic concentration of Sn increases and more atoms of tin are available to form the  $\text{SnS}_2$  compound; hence,  $R_d$  increases.

**Region II.**—Here two different materials are growing at the same time. The jump in  $R_d$  showed at the transition point around  $g = 0.2$  can be explained by considering that the measured film thickness corresponds to both  $\text{SnS}_2$  and  $\text{Sn}_2\text{S}_3$ . In this region, more precursors of tin-bearing species are involved in the growth process because the  $\text{SnCl}_4$  concentration increases. Thus a trend toward an increase in  $R_d$  is expected, but due to the growth competition between both compounds, the effect is not very pronounced.

**Region III.**—Here for specific values of  $g$ , a specific compound was obtained. For  $g = 0.49$ , the deposited material is  $\text{Sn}_2\text{S}_3$  and the

measured film thickness corresponds only to this compound. Thus, a reduction in  $R_d$  from the previous value for  $g$  is expected. For  $0.49 < g < 0.6$ , the deposited material is mainly  $\text{SnS}_2$ , and the measured film thickness corresponds to this compound. Thus, the value of  $R_d$  in this interval must be lower than the one found in the interval discussed for the case of Region II, but would follow the observed increasing trend due to the increase in the concentration of  $\text{SnCl}_4$ .

**Region IV.**—In this region there is the formation of a mixture of different compounds as shown in Fig. 8. The deposition rate shows a small increasing trend due to the incorporation of several compounds.

All the data points shown in Fig. 5 are mean values with the corresponding standard deviation. If this is considered, then in region II, the deposition rate for both compounds is practically independent of the precursor concentrations. Solomon *et al.*<sup>33</sup> reported that, for  $\text{Si}_{1-x}\text{C}_x$  thin films prepared by the decomposition of a mixture of  $\text{SiH}_4$  and  $\text{CH}_4$  by PECVD, the deposition rate is independent of the silane concentration as a consequence of the low power regimen conditions (silane is decomposed by the plasma while methane is not). The conditions reported in this work are similar to that in Ref. 33, thus, a similar behavior is expected. Nevertheless, the chemical reactions are not the same for different precursors, and hence, distinct results may be obtained. This is evident in the case of other  $g$  regions for which the main compound deposited is  $\text{SnS}_2$ . In those regions, a linear relationship between the deposition rate and the  $\text{SnCl}_4$  concentrations may be obtained. Further work in this direction will be carried out in order to confirm this observation.

## Conclusions

This work presents a systematic study on the deposition and structural properties of  $\text{Sn}_x\text{S}_y$  thin film materials prepared by PECVD using  $\text{SnCl}_4$  and  $\text{H}_2\text{S}$  as precursor materials and  $\text{H}_2$  as diluent. It was found that a "low-pressure" regime for which the plasma decomposes  $\text{H}_2\text{S}$  does not decompose  $\text{SnCl}_4$ . The chemical reactions used to explain the film formation were separated from the complicated chemistry of plasma owing to the difference in the decomposition thresholds between both precursors. In this regime  $g$  determines the relative chemical composition, the crystallinity, and the preferential growth of the deposited  $\text{Sn}_x\text{S}_y$  thin films. These films are of polycrystalline nature for all the  $g$  values considered here. For  $g < 0.2$ , EDS measurements have shown that the deposited material is tin disulfide with a stoichiometry close to 1:2. XRD measurements show that this compound presents only the 2H- $\text{SnS}_2$  phase with a hexagonal structure showing a preferential growth along the [001] direction, and hence, the  $c$  axis is perpendicular to the plane of the substrate. All these films present a very smooth surface and high structural quality. For  $g > 0.2$ , XRD measurements show that the deposited material is a mixture of  $\text{SnS}_2$  and  $\text{Sn}_2\text{S}_3$  compounds. It was found that for  $g = 0.49$  the deposited material is mainly  $\text{Sn}_2\text{S}_3$ . The precursor concentrations do not affect the crystalline grain size of the  $\text{SnS}_2$  compound. However, the deposition rate depends on the  $g$  value, because the deposited film is composed of different materials and phases. The maximum deposition rate found for the  $\text{SnS}_2$  compound was 8 nm/min, while for films having the mixture of  $\text{SnS}_2$ - $\text{Sn}_2\text{S}_3$ , it is of the order of 35 nm/min. On the other hand, it was found that the prepared thin films with  $g > 0.1$  have chlorine incorporation, even though small. The hydrogen flow rate added during the process has a gettering type of action, reacting with the chlorine related species generated. However, this effect was not enough to avoid the Cl incorporation at the deposited thin films. More work is necessary to establish the deposition parameters for producing thin films without chlorine. Here, we found specific deposition conditions that lead the  $\text{SnS}_2$  thin film grows with a columnar oriented growth along the  $c$  axes with a deposition rate of 8 nm/min. The crystal grain size of such films is 13 nm. Due to the fact that the  $\text{SnS}_2$  thin films prepared under this condition had shown an n-type electrical conductivity, this work opens up the opportunity to use this material for building an n- $\text{SnS}_2$ /p- $\text{SnS}$  heterojunction prepared completely by PECVD.

### Acknowledgments

We wish to thank Leticia Baños (IIM-UNAM) for XRD analysis, and Jose Guzman (IIM-UNAM) for SEM and EDS analyses. One of the authors (A.S.-J.) is thankful to the PADEP-UNAM program for the financial support given through project no. 5338 in the initial stage of the work. CONACyT, Mexico, has supported this work under contract 3723-PA.

CONACyT (project 3723-PA) Mexico, and Universidad Nacional Autonoma de Mexico assisted in meeting the publication costs of this article.

### References

1. E. Mooser and W. B. Pearson, *Phys. Rev.*, **101**, 492 (1956).
2. G. Busch, C. Frohlinch, and F. Hulliger, *Helv. Phys. Acta*, **34**, 359 (1961).
3. W. Albers, C. Hass, H. J. Vink, and J. D. Wasscher, *J. Appl. Phys. Suppl.*, **32**, 2220 (1961).
4. G. Valiukonics, D. A. Guseinova, G. Krivaite, and A. Sileica, *Phys. Status Solidi B*, **135**, 299 (1990).
5. M. T. S. Nair and P. K. Nair, *J. Phys. D: Appl. Phys.*, **24**, 83 (1991).
6. N. Koteswara Reddy and K. T. Ramakrishna Reddy, in *Proceedings of the IEEE 26th Photovoltaic Specialist Conference*, 515 (1997).
7. G. Domingo, R. S. Itoga, and C. R. Kannewurf, *Phys. Rev.*, **143** (2), 536 (1997).
8. E. Schonerr and W. Stetter, *J. Cryst. Growth*, **30**, 96 (1975).
9. T. Chattopadhyay, J. Pannetier, and H. G. von Schnering, *J. Phys. Chem. Solids*, **44**, 879 (1986).
10. J. George and C. K. Valsala Kumari, *J. Cryst. Growth*, **63**, 233 (1983).
11. K. Kourtakis, J. DiCarlo, R. Kershaw, K. Dwight, and A. Wold, *J. Solid State Chem.*, **76**, 186 (1988).
12. S. K. Arora, D. H. Patel, and M. K. Agarwal, *J. Mater. Sci.*, **29**, 3979 (1994).
13. R. D. Engelken, H. E. McCloud, C. Lee, M. Slayton, and H. Ghoreishi, *J. Electrochem. Soc.*, **134**, 2696 (1987).
14. M. T. S. Nair and P. K. Nair, *Semicond. Sci. Technol.*, **6**, 132 (1991).
15. S. López and A. Ortíz, *Semicond. Sci. Technol.*, **9**, 1 (1994).
16. S. López, S. Granados, and A. Ortíz, *Semicond. Sci. Technol.*, **11**, 433 (1996).
17. N. Koteswara Reddy and K. T. Ramakrishna Reddy, *Thin Solid Films*, **325**, 4 (1998).
18. A. Ortíz, J. C. Alonso, M. Garcia, and J. Toriz, *Semicond. Sci. Technol.*, **11**, 243 (1996).
19. W. Albers, C. Hass, and F. van der Maesen, *J. Phys. Chem. Solids*, **15**, 306 (1960).
20. J. J. Lofersky, *J. Appl. Phys.*, **27**, 77 (1956).
21. M. Parenteau and C. Carbone, *Phys. Rev. B*, **41**, 5227 (1990).
22. R. Whitehouse and A. A. Balchin, *J. Cryst. Growth*, **47**, 203 (1979).
23. G. Said and P. A. Lee, *Phys. Status Solidi A*, **15**, 99 (1973).
24. M. A. Lieberman and A. L. Lichtenberg, *Principles of Plasma Discharges and Materials Processing*, John Wiley & Sons, Inc., New York (1994).
25. A. Von Engel, *Ionized Gases*, 2nd ed., Clarendon Press, Oxford, U.K. (1965).
26. *CRC Handbook of Chemistry and Physics*, 71st ed., D. R. Lide, Editor, CRC Press, Boca Raton, FL (1991).
27. J. C. Alonso, R. Vazquez, A. Ortíz, and V. Pankov, *J. Vac. Sci. Technol. A*, **16**, 1 (1998).
28. I. Traus and H. Suhr, *Plasma Chem. Plasma Process.*, **12**, 275 (1992).
29. H. P. Klug and L. E. Alexander, *X-Ray Diffraction Procedures for Polycrystalline and Amorphous Materials*, John Wiley & Sons, Inc., New York (1954).
30. T. Shibata, Y. Muranushi, T. Miura, and T. Kishi, *J. Mater. Sci.*, **26**, 5107 (1991).
31. S. C. Ray, M. K. Karanjai, and D. DasGupta, *Thin Solid Films*, **350**, 72 (1999).
32. C. Wang and R. G. Cheng, *Philos. Mag. B*, **53**, 183 (1986).
33. I. Solomon, M. P. Schmidt, and H. Tran-Quoc, *Phys. Rev. B*, **38**, 9895 (1988).
34. Z. Zainal, M. Z. Hussein, and A. Ghazali, *Sol. Energy Mater. Sol. Cells*, **40**, 347 (1996).
35. B. Chapman, *Glow Discharge Processes: Sputtering and Plasma Etching*, John Wiley & Sons, Inc., New York (1980).
36. I. Trauss, H. Suhr, J. E. Harry, D. R. Evans, and E. Andrade, *Plasma Chem. Plasma Process.*, **13**, 77 (1993).